Appl. Phys. B 68, 663–669 (1999) / DOI 10.1007/s003409901366

Applied Physics B
Lasers
and Optics

High-efficiency 2 kW XeCl excimer laser

K. Haruta[1], Y. Saito[2], M. Inoue[2], Y. Sato[2], S. Fujikawa[2], A. Suzuki[2], H. Nagai[3]

[1] Vision 21 New Business Development Center, Mitsubishi Electric Corporation, 2-2-3 Marunouchi Chiyoda-ku, Tokyo 100, Japan
(Fax: +81-3/3218-3124, E-mail: harutaky@ebd.hon.melco.co.jp)
[2] Advanced Technology R&D Center, Mitsubishi Electric Corporation, 8-1-1 Tsukaguchi-honmachi, Amagasaki 661, Japan
[3] Corporate Total Productivity Management & Environmental Programs, Mitsubishi Electric Corporation, 2-2-1 Minatomirai Nishi-ku, Yokohama, Kanagawa 220-81, Japan

Received: 15 May 1998/Revised version: 5 August 1998/Published online: 24 February 1999

Abstract. An average power of 2 kW with an efficiency of 4.3% was demonstrated in a discharge-pumped XeCl laser using a spiker/sustainer circuit and surface corona preionizer. Effective discharge volume is 4 cm gap length, 2.5 cm discharge width and 2 m effective discharge length. The behavior of the 500 W laser developed in previous work was investigated by computer simulation. It was found that most of the spiker energy is not deposited into the discharge volume in the reverse voltage operating mode, though this operating mode is indispensable for high repetitive operation of the spiker/sustainer circuit. Based on the simulation results, the laser apparatus was redesigned and consequently a laser output energy of 2.5 J with a high efficiency of 4.5% obtained. In repetitive operation at 800 Hz, the high performance mentioned above was attained.

PACS: 42.55

Excimer lasers are expected to serve as new manufacturing tools in the next century, and industrial applications for micro-lithography, micron-sized hole drilling, laser ablation, and surface annealing are actually increasing. Under these conditions, interest in the development of a high-power excimer laser has been increasing. In the middle of the 1980s, two national projects were started concurrently in Europe and Japan to spur innovation in processing technologies for the next century. Technologies concerning the high-power excimer laser made remarkable progress in these projects. In the European "EUREKA project", a XeCl excimer laser with an average power of 750 W was reported in 1990 [1] and an average power of 1 kW at a repetition rate of 100 Hz was reported using an X-ray preionized XeCl excimer laser in 1993 [2]. In 1998, Timmermans reported an X-ray-preionized 1 kW XeCl laser for laser ablation processing [3].

In 1994, we also demonstrated a 2 kW high-power XeCl laser under the Japanese “AMMTRA project” [4]. In this laser, a new combination system of surface corona discharge preionizer and spiker/sustainer excitation circuit was used. The surface corona discharge preionizer had been developed because of the following advantages. It easily provides a larger discharge volume than a conventional arc discharge preionizer. It is also more suitable for repetitive operation near 1 kHz than an X-ray preionizer. The spiker/sustainer excitation circuit was adopted in order to realize a high average power of 2 kW with a high efficiency of near 4%. The spiker/sustainer circuit was first demonstrated by Long et al. [5] and improved by Taylor et al. [6], Fisher et al. [7], and Timmermans et al. [8]. The spiker circuit acts only to initiate discharge and reduce the discharge impedance to a quasisteady-state value. The main energy for excitation is then delivered from the sustainer circuit to the discharge volume under impedance-matching conditions. The efficient energy delivery from the excitation circuit results in a high efficiency of more than 4% at a laser output of 2–4 J [5–8]. However, these studies were done in a single-shot operation. It was found in our study that the conventional operating mode for the spiker/sustainer circuit was not suited for high repetitive operation. We developed a new operating mode (reverse voltage mode) and a technique for controlling preionization timing to achieve high repetitive operation. As a result, 2 kW average power (2.6 J/pulse) was enabled at a repetition rate of 800 Hz. However, the total efficiency was confined to a low value of 2.8% [4].

In this study, the characteristics of this laser were investigated by computer simulation and the laser was subsequently redesigned based on simulation results. A high-efficiency and high power excimer laser is reported as a result of these improvements.

1 Experimental apparatus

1.1 Configuration of XeCl *laser*

The electrode system is the same as reported in the previous paper [4]. The main electrodes consist of a Chang-profile electrode and a perforated plate electrode. The perforated plate electrode is also used for surface corona discharge preionization together with a dielectric (alumina ceramic

pipe) and an auxiliary electrode. The top surface of the alumina pipe is flattened in order to contact the perforated plate electrode. The auxiliary electrode has a semicylindrical shape and is located inside the pipe. When a high voltage pulse is applied between the perforated plate electrode and the auxiliary electrode, a corona discharge is formed in each perforation of the perforated plate electrode. Uniformity of the corona discharge is maintained over the perforated plate electrode by the capacitive ballast effect of the alumina ceramic. The corona discharge seeds electrons ever the surface of the perforated plate electrode. In the following stage, the seeded electrons increase quickly by electron avalanche in the electric field between the main electrodes. When the density of electrons increases enough to cause the gas breakdown, the uniform main discharge is formed. The optimum area percentage for openings in the perforated electrode was determined to be 40%–50% based on laser output performance and discharge stability [4].

The excitation circuit is shown in Fig. 1. The spiker circuit is a conventional charge-transfer type. The capacitance of primary and secondary capacitors are 12 nF and 9.7 nF, respectively. A pulse-forming line was adopted as the sustainer circuit, which consists of coaxial-type capacitors connected two in series and eighteen in parallel. The total capacitance is 520 nF and the structural inductance is about 6 nH. The charging voltage of the sustainer circuit was changed from 6 kV to 10 kV. The maximum charging voltage is limited to 10 kV by the self-breakdown between the main electrodes. A racetrack-shaped magnetic switch is used to stop the current flow from sustainer circuit to the main electrodes during operation of the spiker circuit. The core of the switch is made of a cobalt-based alloy. The maximum change of flux density, path length, and total cross section of the magnetic switch are 1.1 T, 1.4 m, and 15 cm^2, respectively.

The operation mode of the circuit is the reverse voltage mode [4]. First, the spiker circuit pulls the gap voltage (V_{gap}) to the opposite side from sustainer voltage. The magnetic switch is designed to saturate before the voltage, V_{gap}, reaches the gas breakdown point. As soon as the magnetic switch saturates, the charge on the large capacitor of the sustainer circuit (C_{sus}) is quickly transferred to the small capacitor of the spiker circuit ($C_{1,sp}$). This charge transfer reverses V_{gap} and generates a quite steep voltage rise of nearly 1000 kV/μs. This rate is several times larger than that of conventional charge-transfer circuits and it very effectively initiates homogeneous discharge. Gas breakdown starts just before the first peak of the reverse voltage and spiker-discharge is formed. Because the magnetic switch is already saturated, the current starts to flow into the discharge region from the sustainer capacitor following the spiker discharge without any delay time. A homogeneous and stable discharge is then maintained for several hundred nanoseconds. In the usual operation mode, the spiker circuit initiates gas breakdown, after which the magnetic switch saturates. Because of the limited switching time of the magnetic switch, a delay time is generated between spiker discharge and sustainer discharge. As a result, the spiker discharge becomes inhomogeneous during this delay time and a stable main discharge can no longer be formed, especially in the case of high repetitive operation.

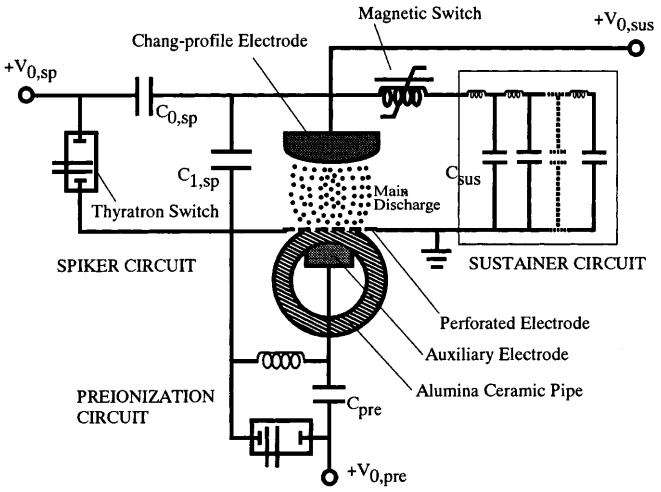

Fig. 1. Excitation circuit

The laser gas composition is Xe 0.24%/HCl 0.03%/Ne buffer (total pressure is 0.33 MPa).

These configurations are the same as that of the 500 W laser reported previously [9] (described as "500-W-type laser" after this). In addition, the experimental apparatus was modified as follows.

(i) The oil-cooling jacket of the thyratron switch was changed to a cylindrical type so that the current loop formed a coaxial line. This structure is very effective in reducing the stray inductance.
(ii) The spiker circuit was redesigned to decrease stray inductance as much as possible based on the static electrical field analysis for dielectric breakdown.
As a result of modifications described in (i) and (ii), the spiker inductance was reduced from 750 nH to 250 nH.
(iii) Effective discharge length was extended up to 2 m, while the gap length and discharge width are 40 mm and 20 mm, respectively. It was quite exacting to process the 2-m straight alumina ceramic pipe for the surface corona preionizer. Then, two sets of electrodes with a discharge length of 1 m were installed in series in the laser vessel. A distance of 40 mm is necessary for insulation between two sets of electrodes. This increases the resonator length to 3.1 m.
(iv) The maximum gas velocity in the discharge zone was increased from 50 m/s to 80 m/s for high repetitive operation. The clearance ratio is 4–5.

1.2 Simulation program of XeCl *laser*

Maeda et al. [10], Kannari et al. [11], and Hokazono et al. [12] detailed the simulation code for a self-sustained discharge excimer laser with a charge-transfer-type excitation circuit. We extended this program to apply the code to a high-power XeCl laser with spiker/sustainer circuit [9]. The configuration of simulation code described here is basically the same as that reported before [9] except for the following modifications.

(i) The magnetic switch was treated as an ideal switch in the previous program. In the new program, the nonlinear inductance of the magnetic switch is described by an empirical formula. Figure 2 shows the measured characteristics of the high-frequency magnetic saturation and

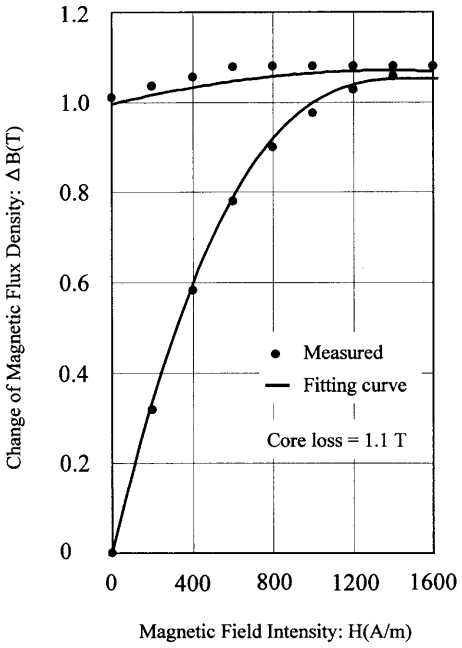

Fig. 2. Characteristics of high-frequency magnetic saturation of magnetic switch

fitting curve. The tangent of the fitting curve corresponds to the inductance of the magnetic switch. Increasing leak current (= path length of magnetic switch × H) from sustainer capacitor (C_{sus}) to spiker capacitor ($C_{1,sp}$), the inductance of the magnetic switch is gradually reduced during the spiker operation stage. When the leak current reaches about 1.4 kA, a rapid drop of inductance occurs, that is, switching starts and the inductance quickly reaches a minimum value of 6.9 nH.

(ii) The photon density was assumed to be the same over the whole optical path in the previous program. Our program adopts equations for light propagation for the calculation of laser power; the laser output energy is calculated by solving three simultaneous equations comprised of the rate equation for XeCl* and equations of light propagation ((1) and (2)).

$$\frac{\partial N_{ph}^{+}}{\partial t}+\frac{\partial N_{ph}^{+}}{\partial x}=c\sigma_m N_m N_{ph}^{+}+\alpha\frac{N_m}{\tau_m}-\sum c\sigma_n^{i} N_i N_{ph}^{+}\,. \quad (1)$$

$$\frac{\partial N_{ph}^{-}}{\partial t}+\frac{\partial N_{ph}^{-}}{\partial x}=c\sigma_m N_m N_{ph}^{-}+\alpha\frac{N_m}{\tau_m}-\sum c\sigma_n^{i} N_i N_{ph}^{-}\,. \quad (2)$$

N_{ph}^{+} : photon density propagated to the partial reflector ,
N_{ph}^{-} : photon density propagated to the total reflector ,
σ_n^{i} : cross section of photo-absorption by species “i” ,
α : proportion of spontaneous emission that contributes to laser power .

These modifications bring the simulation code close to modeling the actual laser system.

The simulation code consists of a circuit equation, a steady-state Boltzmann equation, and rate equations. Zero-dimensional uniform discharge plasma without streamer, arcing or uneven distribution of electrons is assumed. In addition, cathode drop is disregarded because the voltage between electrodes is quite large as compared with that of cathode drop and also the length of the cathode sheath is negligibly small compared to gap length. Breakdown is assumed to be caused only by self-avalanche electron multiplication.

The equivalent circuit model and circuit parameters adopted in circuit equation are shown in Fig. 3 and Table 1, respectively. Based on the measurement results, the resistance of the thyratron switch is programmed to be changed from 0.5 Ω to 2.5 Ω for reversed current flow. This is because the glow mode connection of the thyratron switch changes to the arc mode for reverse current flow.

Table 1. Circuit parameters adopted in simulation program

$C_{0,sp}$ / $C_{1,sp}$	12 nF / 9.7 nF
C_p / L_p / C_{sus}	104 nF / 2.5 nH / 104 × 5 = 520 nF
L_1 / L_2+L_d / L_s+L_t	250 nH / 7.5 nH / 45 nH
R_1 / R_s	0.5(2.5)Ω / 0.05 Ω

Eighty reactions are taken into account for thirty-six species in the rate equations. For example, the rate equations for electron and XeCl* are as follows.

$$\frac{dN_e}{dt}=\sum k_{ei}N_i N_e+\sum k_{pe}N_i N_j+\sum\frac{N_j}{\tau_j}+\sum c\sigma_j N_j N_{ph}-\sum k_a N_j N_e\,. \quad (3)$$

$$\frac{dN_m}{dt}=\sum k_{jk}N_j N_k+c\sigma_n N_n N_{ph}-\sum k_j N_j N_e-\sum k_j N_j N_k-\sum k_j N_j N_k N_l-\frac{N_m}{\tau_m}-c\sigma_m N_{ph} N_m\,. \quad (4)$$

N_e : electron density , N_{ph} : photon density ,
N_i, N_j, N_k, N_l : density of atom or molecule ,
N_n : density of Xe_2Cl^* , N_m : density of XeCl* ,

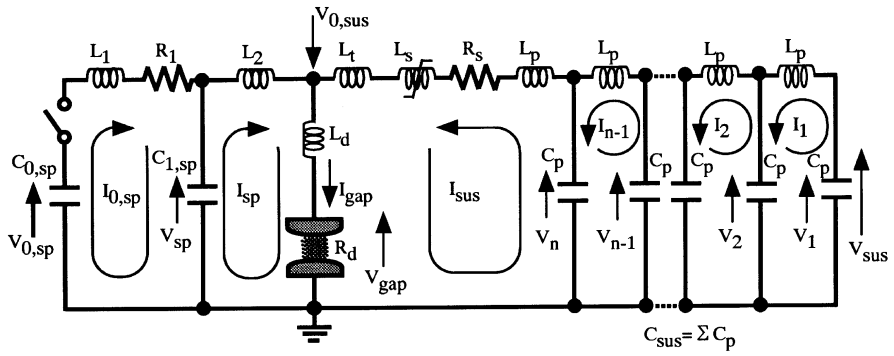

Fig. 3. Equivalent circuit model in simulation code

k_{ei} : rate coefficient of ionization under electron impact ,
k_{pe}: rate coefficient of ionizing collision (e.g. Penning ionization) ,
k_a : rate coefficient of electron attachment (e.g. dissociative attachment by HCl) ,
k_{jk} : rate coefficient of exciting collision ,
k_j : rate coefficient of quenching reaction ,
τ_j : lifetime for auto-ionization , τ_m : lifetime of $XeCl^*$,
c : speed of light ,
σ_j : cross section of photoionization ,
σ_n : cross section of photo-absorption by Xe_2Cl^* ,
σ_m: cross section of induced emission .

The optimum values of rate constants [11] and cross section of induced emission [12] are taken from among the various reports.

The Boltzmann equation is solved numerically in the two-term approximation to describe the electron collision process in the discharge plasma. Superelastic collision is neglected though it is considered in the rate equation. Electron–electron collision is also excluded [13].

The circuit equation and the rate equation are solved through step-by-step calculation and for every 2% change in the value of E/N, the Boltzmann equation is used for recalculation of rate coefficients and electron mobility. The circuit equation is connected to other equations by the term for resistance in discharge region, R_d,

$$R_d = \frac{d}{eN_eS\mu_e} . \tag{5}$$

R_d : resistance in discharge region, d : gap length,
e : charge of electron, N_e : electron density,
S : cross section of discharge region, μ_e : electron mobility,

where the values of N_e and μ_e are calculated from the rate equations and Boltzmann equation, respectively.

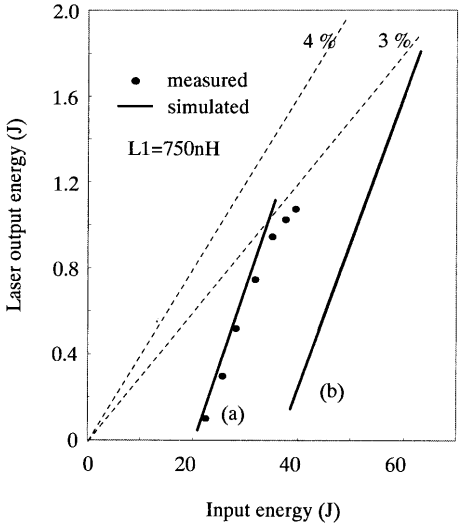

Fig. 4. Laser output of 500-W-type laser: (a) effective discharge length of 1 m, (b) effective discharge length of 2 m

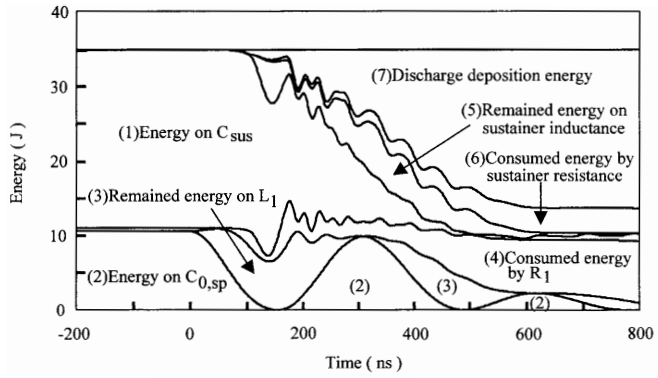

Fig. 5. Simulated energy allocation for 500 W type laser

2 Experimental results

Figure 4 shows the laser output simulation results when the effective discharge length for the 500-W-type laser was extended to 2 m. The actual and simulated results for a discharge length of 1 m are also plotted for reference. The slope efficiency is about 6.8% and is a fairly high value for discharge excitation XeCl lasers. However, as the threshold value increases to 36 J, the total efficiency decreases. As a result, it is difficult to obtain a total efficiency of more than 3%.

Energy allocation for the 500-W-type laser was investigated by simulation. The result is illustrated graphically in Fig. 5, as reported before [14]. Eighty-nine percent of the stored energy of the sustainer capacitor (C_{sus}) is deposited into the discharge volume. On the other hand, most of the stored energy of the spiker capacitor ($C_{0,sp}$) is not deposited into the discharge volume. The figure indicates that the energy of spiker capacitor ($C_{0,sp}$) is transferred to the spiker inductance (L_1) and then most of the energy swings back to the spiker capacitor at a time of 300 ns. In the next step, the energy is transferred again to the spiker inductance. But, the resistance of the thyratron switch changes from 0.5 Ω to 2.5 Ω in response to current reversal after 300 ns and consumes the spiker energy rapidly, before spiker inductance. This energy loss is clearly the main factor of the high threshold value.

From these results, the initial stored energy of the spiker capacitor should be reduced as much as possible in order to increase the total efficiency. For this purpose, the spiker inductance of the experimental apparatus was reduced from 750 nH to 250 nH in the redesign of 500-W-type laser. Figure 6 shows observed waveforms of voltage, current, and laser pulse of the improved laser with the simulation results. The computer simulation is also used to estimate those values that can not be measured actually. The point “a” shows the start of spiker circuit, “b” is the beginning point of gap-voltage reversal, and “c” is the gas breakdown point. As can be seen from the figure, the simulated results are in good agreement with the experimental results. The rise rate of reverse voltage, the gap voltage (V_{gap}) in the “b” – “c” region, is increased from 1020 kV/μs for the 500-W-type laser to 1460 kV/μs, while the spiker charging voltage can be reduced from 42 kV (500-W-type laser) to 30 kV, as reported later. As described in the previous section, the faster voltage rise rate is more effective to initiate the homogeneous and stable discharge. We also found that the amount of filamentation during uniform discharge is apparently decreased, compared with that of the 500-W-type laser. Gas breakdown occurred at a gap voltage

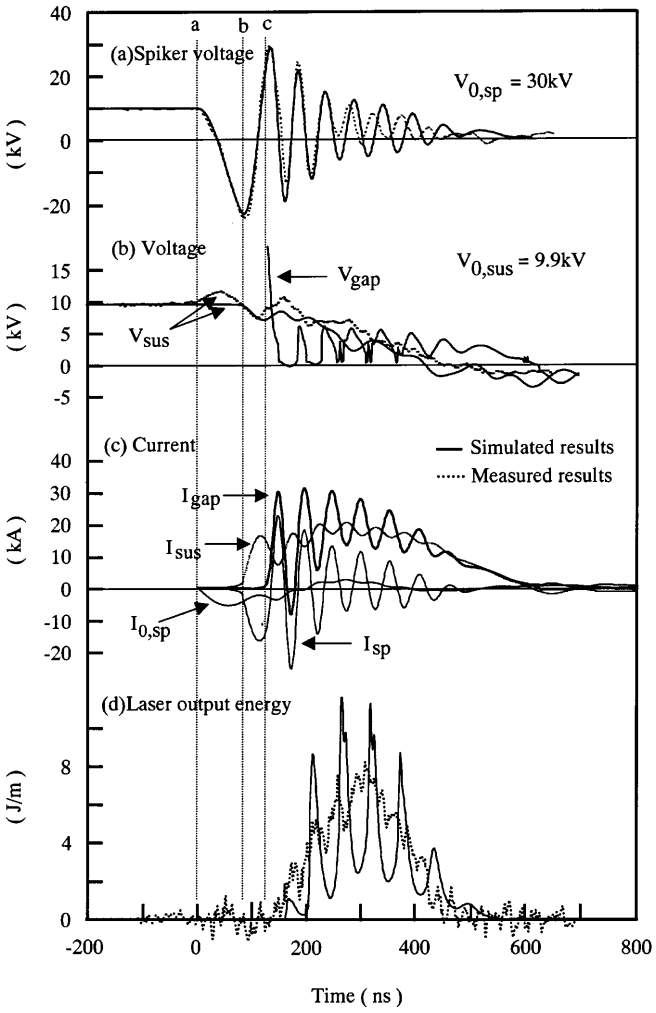

Fig. 6a–d. Measured and simulated characteristics of temporal behavior of improved laser: **a** spiker voltage; **b** sustainer voltage and gap voltage; **c** current; **d** laser output energy

of 21.7 kV. The gap voltage quickly goes down and then oscillates, but an average value is maintained at about 4 kV over a period of about 400 ns. The current characteristic shows that the secondary capacitor ($C_{1,sp}$) of the spiker circuit plays an important role for energy deposition into the discharge volume. The spiker current of the secondary loop (I_{sp}) accounts for more than 85% of discharge current (I_{gap}) in the first spike of discharge and about 70% even in the second spike. It means that a large portion of sustainer circuit energy does not flow directly into the discharge volume, but first transfers to the secondary spiker capacitor ($C_{1,sp}$) and then flows into discharge volume. It is worth noting that the spiker current in primary loop ($I_{0,sp}$) fairly decreases at a point corresponding to the first discharge current spike. This means that a part of the spiker current flows into the discharge plasma. Actually, simulation of energy allocation for the improved laser indicates that 48% of spiker energy is deposited into the discharge volume; the peak current of the first spike of discharge current increases from 24 kA (the case of 500-W-type laser) to 30 kA. The first discharge spike is very effective in raising the gain quickly, and laser oscillation of the improved laser starts about 50 ns earlier than that of the 500-W-type laser after gas breakdown.

The dependency of laser output energy on the charging voltage of the spiker circuit is plotted in Fig. 7. Low charging voltage cannot drag the spiker voltage fully down to the negative side and make the slope of the reverse voltage less steep. On the other hand, a high charging voltage drags the spiker voltage too much and gas breakdown starts in an early stage of voltage reversal where sufficient overvoltage is not supplied to the main electrodes. Thus, the maximum output energy is obtained at a spiker voltage of 30 kV, while an optimum value for initial spiker charging voltage was 42 kV for the 500-W-type laser. This means that the spiker energy of the improved laser can be reduced to 51% ($= (30/42)^2$) of that for the 500-W-type laser.

The dependency of laser output energy on reflectivity of the partial reflector was measured. The optimum reflectivity was found to be 10% from the experimental result, whereas the simulated result gives a value of 25%. This shows that the actual gain in the discharge volume must be higher than the simulated result. The actual net gain was measured by the amplifier method. The ratio of laser input energy E_{in} to saturation energy E_s was plotted against the ratio of output energy E_{out} to saturation energy E_s. The plot gives a value of 3.16 as the straight-line intercept corresponding to gL (g; net gain, L; effective discharge length, 2 m). The net gain was calculated to be 1.58%. On the other hand, the simulated results indicate a small signal gain and absorption loss of about 1%/cm and 0.07%/cm, respectively, slightly lower than the above-measured value. The small signal gain and absorption loss are significantly lower than for conventional lasers with charge-transfer excitation circuits (for example 15% and 0.5%/cm [12]). This is because the partial pressures of Xe and HCl in the laser gas are about one order lower than those of conventional lasers. On the other hand, however, low partial pressure of HCl effectively retards electron attachment, the main process of discharge termination, and makes it possible to realize a long laser-pulse duration.

Laser output energy of the improved laser is plotted in Fig. 8 together with the simulated results. The simulation predicts that the threshold decreases by 36 J to 17 J, whereas the experimental result gives a threshold value of 28 J. The experimental result of the slope efficiency is 9.6%; that is, about 1.7 times larger than the simulated value of 5.7%. These differences are caused from inaccuracy of rate constants of the rate equations in the simulation program. However, the experimental results of laser output are roughly in accord with expectations based on the simulation. The maximum output

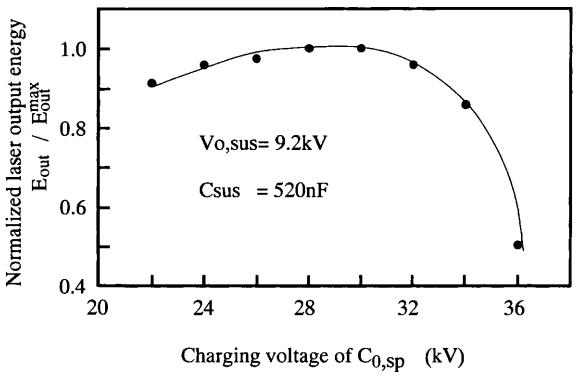

Fig. 7. Dependency of laser output on spiker charging voltage

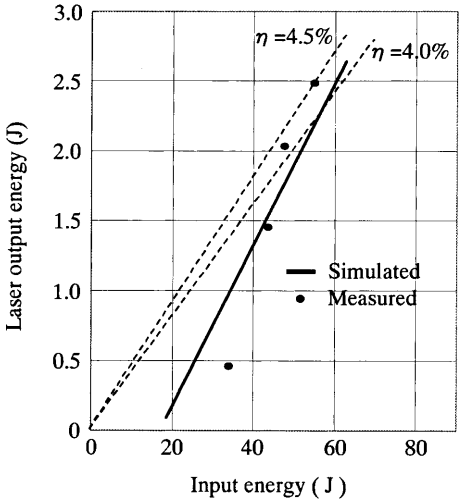

Fig. 8. Laser output energy vs. input energy plot for improved laser

energy of 2.5 J is obtained at an input energy of 55 J. A total efficiency of 4.5% is the highest result yet, as compared with previous reports [5–8]. The output energy decreases at an input energy of more than 60 J. The cause of this has not been elucidated yet, but it is not due to the instability of discharge because the input energy density corresponds to an input energy of 30 J in the 500-W-type laser (discharge length = 1 m), in which case the laser output energy still increased beyond such an input energy density.

In the next step, high repetitive operation was tried. An average power of 2 kW was planned to be attained at a repetition rate of 800 Hz with an output energy of 2.5 J. However, a rapid decrease of laser power was observed. This is due to the deterioration of the laser gas; only by replacing laser gas can the output energy be restored. The average power meter has a time constant of about 2 or 3 s and it can not trace the average power at the early stage of high repetitive operation. Therefore, the laser output energy was monitored shot by shot using a phototube. The reduced average power vs. shot number plot is shown in Fig. 9. The shot-by-shot oscillogram is also shown. Though in a burst mode (less than 10 shots), an average power of 2 kW was obtained with an output energy of 2.5 J at a repetition rate of 800 Hz. At this time, the total input energy was slightly increased to 57.5 J to cover the laser power decrease. The total efficiency is 4.3%.

3 Discussion

Another means of reducing the spiker energy is reducing the capacitance of spiker capacitors. The laser characteristics were simulated for a case in which the capacitance of primary and secondary spiker capacitor are reduced from 12 nF/9.7 nF to 6 nF/4.8 nF, respectively. The simulation result shows that a sufficient rise rate for reverse voltage of 1400 kV/μs is obtained at an initial spiker charging voltage of 30 kV. As a result, about 75% of spiker energy can be eliminated. However, the laser output characteristic is not improved, as shown in Fig. 10. The threshold is somewhat large than in the case of reducing inductance. The slope efficiency is decreased and the laser output energy at an input energy of more than 55 J is predicted to be lower than that of the case where the discharge length of the 500-W-type laser is extended to 2 m. These results are caused by reduction of energy from the secondary capacitor to the discharge volume in the initial stage of discharge. The waveforms for discharge energy and laser pulse are shown in Fig. 11 for each case of reducing inductance and reducing capacitance. As reported in Fig. 6c, the discharge current from the secondary capacitor contributed largely to the first and second spike of discharge current and these spikes are important in raising the gain quickly in the initial stage of laser oscillation. In the case of reducing capacitance, the energy of the first and second spikes is apparently lower than in the reduced inductance case. As a result, laser oscillation starts about 140 ns later from the first peak of discharge energy, whereas it is only 74 ns for the reduced inductance case. Thus, reducing the spiker capacitance is not effective in improving the laser efficiency.

We also tried to improve the total efficiency by increasing the input energy. The initial charging voltage of the sustainer capacitor is limited by the self-breakdown between the main electrodes, as mentioned before. The capacitance of the sustainer capacitor was increased to increase the input energy. As a result, the plot of laser output energy vs. input energy shifts toward a high threshold value, while the slope efficiency is almost same. The laser output energy slightly in-

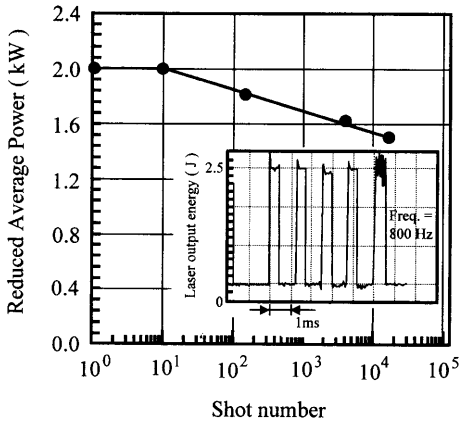

Fig. 9. Dependency of laser output energy on shot number

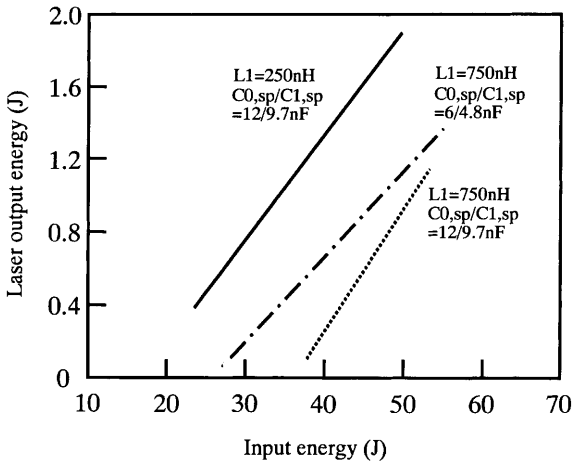

Fig. 10. Simulated laser output for the case of reducing spiker capacitances

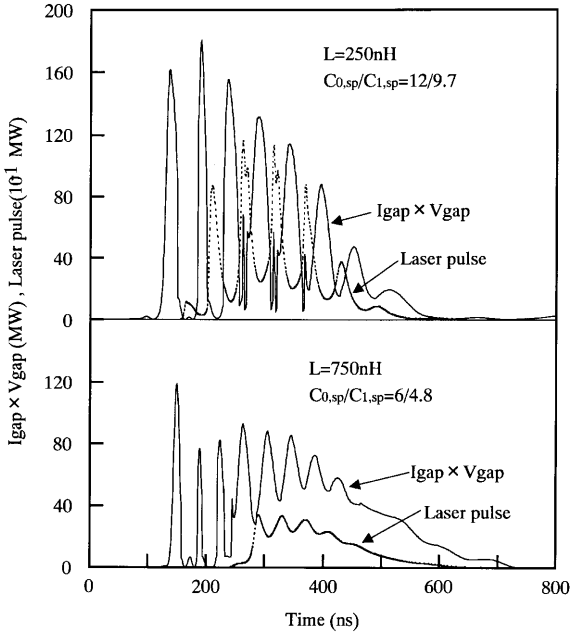

Fig. 11. Waveforms of discharge energy and laser pulse

creased but the total efficiency is not improved. The reason is as follows: the larger the sustainer capacitance becomes, the lower the charging voltage needed to attain the same input energy. The sustainer charging voltage strongly affects the breakdown voltage in the voltage reversal process, and a low sustainer charging voltage reduces the breakdown voltage. Then, the impedance of the discharge volume decreases more slowly after gas breakdown. This effect results in a delay of the beginning of laser oscillation and, consequently, in an increase of the threshold in the laser output vs. input energy plot.

4 Conclusion

The discharge behavior of a prototype 500 W laser was investigated analytically, the results showing that most of the spiker energy is not used for discharge, but is consumed by the resistance of the spiker loop between primary and secondary capacitors. This phenomenon is peculiar to the reverse voltage mode. The reverse voltage mode possesses superiority for stability and homogeneity of discharge; however, on the other hand, it has the disadvantage of wasting spiker energy. The initial stored energy of the spiker capacitor should therefore be reduced as much as possible in order to increase the total efficiency.

It is found from the simulation results that the most effective means of cutting down this energy loss is to reduce the spiker inductance. A decrease of the spiker capacitance or increase of the input energy from the sustainer capacitor is not effective in improving the total efficiency. On the basis of these estimations, the spiker inductance of the experimental apparatus was reduced from 750 nH to 250 nH by modifying a 500-W-type laser. A maximum laser output energy of 2.5 J was obtained with a total efficiency of 4.5%. Next, high repetitive operation was tried and an average power of 2 kW obtained with output energy of 2.5 J at a repetition rate of 800 Hz. At this time, a total efficiency of 4.3% was obtained. We reported a 2 kW XeCl laser with an efficiency of 2.8% previously, using 3-stage tandem configuration (effective discharge length = 3 m [4]). In this experiment, both a high power of 2 kW and high efficiency of more than 4% were achieved even with a shorter discharge length of 2 m. Though this result was obtained only in a burst mode because of the gas deterioration, it points to the development of a high-efficiency, high-power excimer laser.

Acknowledgements. This work was supported in part under the program "Advanced Material-Processing and Machining System" consigned to the Advanced Material-Processing and Machining Technology Research Association from the New Energy and Industrial Technology Development Organization, which was carried out under the Industrial Science and Technology Frontier Program enforced by the Agency of Industrial Science and Technology, the Ministry of International Trade and Industry.

References

1. E. Muller-Horsche, P. Oesterlin, D. Basting: Proc. High-power Gas Lasers 1990, Los Angeles, CA **1225**, 142 (1990)
2. B. Godard, P. Murer, M. Stehle, J. Bonnet, D. Pigache: CLEO'93, Baltimore, Maryland, CTh11 (1993)
3. J.C. Timmermans: Proc. of SPIE, High-power Laser Ablation 1998, Santa Fe, April 26-30, **3343**, 56 (1998)
4. K. Haruta, Y. Sato, M. Inoue, A. Suzuki, S. Fujikawa, Y. Saito: Final Report of Advanced Material-Processing and Machining technology Research Project, I-1-1 (1994);
   Y. Sato, M. Inoue, S. Fujikawa, Y. Saito, A. Suzuki, K. Haruta, H. Nagai: IEEE J. Selected topics QE **1** (3), 811 (1995)
5. W.H. Long, Jr., M.J. Pummer, E.A. Stappaerts: Appl. Phys. Lett. **43**, 735 (1983)
6. R.S. Taylor, K-E. Leopold: Appl. Phys. Lett. **46**, 335 (1985)
7. C.H. Fisher, M.J. Kushner, T.E. DeHart, J.P. McDaniel, R.A. Petr, J.J. Ewing: Appl. Phys. Lett. **48**, 1574 (1986)
8. J.C.M. Timmermans, F.A. van Goor, W.J. Witteman: Appl. Phys. B **57**, 441 (1993)
9. Y. Saito, Y. Sato, S. Fujikawa, M. Inoue, K. Haruta: Trans. IEE of Japan, **116-A** (4), 297 (1996)
10. M. Maeda, A. Takahashi, T. Mizunami, Y. Miyazoe: Jpn. J. Appl. Phys. **21** (8), 1161 (1982)
11. F. Kannari, W.D. Kimura, J.J. Ewing: J. Appl. Phys. **68** (6), 2615 (1990)
12. H. Hokazono, K. Midorikawa, M. Obara, T. Fujioka: J. Appl. Phys. **56**, (3), 680 (1984)
13. A.E. Green, C.A. Brau: IEEE J. Quantum Electron. **QE-14**, 951 (1978)
14. Y. Saito, Y. Sato, S. Fujikawa, M. Inoue, K. Haruta: Proc. of SPIE, The International Society for Opt. Engineering, San Jose, Feb. 12-13, 1997, **2989**, 183 (1997)